Vibrating Target Micro-Doppler Signature in Bistatic SAR With a Fixed Receiver

Carmine Clemente, *Student Member, IEEE*, and John J. Soraghan, *Senior Member, IEEE*

***Abstract*—Bistatic synthetic aperture radar (BSAR) provides strategical, technical and economical advantages in radar imaging. Motions and micro-motions of objects in an illuminated scene introduces Doppler and micro-Doppler effects in the received radar echoes. Combining the advantages introduced by the bistatic configuration and the usefulness of the micro-Doppler signature characterization will provide a powerful tool for military and civil remote sensing applications such as target recognition and classification. In this paper, a vibrating micro-Doppler signature for a BSAR system with fixed receiver is analyzed and compared to the signature obtained in a monostatic SAR system. The micro-Doppler effect is derived for a vibrating target in the bistatic SAR. The corresponding bistatic factor is shown to be a function of the bistatic acquisition geometry. Also, the effect of the target vibration on the focused image is shown to be influenced by the acquisition geometry. The derived model is useful for micro-Doppler classification. Simulations for 94 GHz and 10 GHz are given and the results confirm the derived model.**

***Index Terms*—Bistatic SAR, micro-doppler signature, synthetic aperture radar (SAR), time-frequency analysis, vibrating target.**

I. Introduction

BISTATIC synthetic aperture radar (BSAR) operates with a separate transmitter and receiver introducing new characteristics compared to traditional monostatic SAR systems [1]. Some of the advantages of the bistatic configuration include i) the reduction of vulnerability of the system in military applications with the ability of having the transmitter located at safe distance from a the hostile area; ii) the capability for the bistatic system to be employed for imaging in the flight direction or backwards in flight assistance systems; iii) reduction of costs; iv) measurement of the bistatic clutter characteristic and; v) the reduction of the dihedral and polyhedral effects in urban areas improving the images quality. These advantages encouraged the remote sensing community to conduct new bistatic experiments with different configurations [2]–[7], that provided interesting results in terms of resolution and target detection. A common problem in SAR systems is the detection and the characterization of moving targets within a scene. If the target exhibits a regular and straight motion pattern during the image acquisition then a ground moving target indicator (GMTI) is a normally used technique. The remote sensing community have proposed processing techniques for moving target in the bistatic case [8]–[10]. However, characterizing target movement is generally different from the constant or linear motion observed in the GMTI [11]. Vibrations and rotations of the target characterize a specific target. The ability to identify and classify these kind of motions allow us to classify the target. For example vibrating micro-Doppler signatures allow us to distinguish a diesel engine of a bus from a gas turbine engine of a tank [12], [13].

In [14] the micro-Doppler signature for vibrating targets in a monostatic SAR system was analyzed and tested with an X-band system, while in [15] the micro-Doppler for vibrating and rotating SAR was analyzed and tested with a millimeter Wave (mmW) system. In both cases time-frequency analysis was performed using the Wigner Ville Distribution exploiting the properties of the Cohen's family of transforms [16].

In this paper, the vibration effect on the received echoes for a bistatic SAR system with fixed recevier is modeled. The pseudo-Wigner Ville distribution (PWVD) is used to analyze simulated data for X-band and mmW systems. The bistatic SAR configuration was never considered before, and a model for the micro-Doppler signature was not suitable. Also, the effect on the focused image changes with the bistatic geometry was not considered in the analysis in [12], which considered only the monostatic case. The remainder of paper is organized as follows. In Section II, possible applications of the micro-Doppler signature in remote sensing are introduced. In Section III, the bistatic SAR geometry and the received signal model are discussed. In Section IV, the micro-Doppler effect from a vibrating target in the bistatic geometry is introduced and analyzed, the effect on the focused image of the bistatic geometry and of the limitations on the system Doppler bandwidth are investigated. Section V presents simulation results of focused vibrating target and PWVDs of the received echoes compared with the analytical expected signature and the signature obtained with a monostatic system.

II. Applications of Micro-Doppler Signature From Bistatic SAR

The knowledge of micro-Doppler signature is of interest for remote sensing applications [17]. Micro-Doppler signature is the description of details of a target. For this reason, the micro-Doppler signature is a potential rich source of information that can be used for a variety of applications.

Manuscript received April 26, 2011; revised October 10, 2011; accepted December 11, 2011. Date of publication February 3, 2012; date of current version July 18, 2012. This work was supported by the Engineering and Physical Research Council (Grant N. EP/H012877/1), the MOD University Defence Research Centre in Signal Processing and Selex-Galileo Edinburgh.

The authors are with the Centre for Excellence in Signal and Image Processing, Department of Electronic and Electrical Engineering, University of Strathclyde, G1 1XW Glasgow, U.K. (e-mail: carmine.clemente@eee.strath.ac.uk; j.soraghan@eee.strath.ac.uk).

Color versions of one or more of the figures in this paper are available online at http://ieeexplore.ieee.org.

Digital Object Identifier 10.1109/TGRS.2011.2180394

A. Target Recognition

Micro-Doppler can be regarded as a unique signature of the target that provides additional information about the target that is complementary to existing methods. Specific applications include the recognition of space, air, and ground targets. For example, the micro-Doppler effect can be used to identify specific types of vehicles and determine their movement and the speed of their engines. Vibrations generated by a vehicle engine can be detected by radar signals returned from the surface of the vehicle. For example, from micro-Doppler modulations in the engine vibration signal, one can distinguish whether it is a gas turbine engine of a tank or the diesel engine of a bus. The outfield measurement of ground targets indicates that micro-Doppler signatures have great significance for vehicle recognition. Micro-Doppler signature can also be used for human identification at a distance since radar has the advantage of detecting and identifying humans at distances in all weather conditions at day or night.

B. Micromotion Detection

Existing methods for searching and rescuing human victims buried under earthquake rubble or collapsed building debris are the utilization of dogs, seismic, or optical devices. These existing devices are not effective if the rubble or debris covering the human victims is thicker than a few feet, particularly for the case when the victims are completely trapped or too weak to respond to signal sent by the rescuers. As the development of life-detection system, microwave, and laser can be used to detect the breathing and heartbeat signals of passive victims who are completely trapped or too weak to respond to the existing seismic detection system. The basic physical principle for the operation of a microwave lifedetection system is rather simple. When a microwave beam of appropriate frequency (L or S band) is aimed at a pile of earthquake rubble or collapsed building debris under which a human subject is buried, the microwave beam can penetrate through the rubble or the debris to reach the subject. When the human subject is illuminated by the microwave beam, the reflected wave from the subject will be modulated by the subject's body movements, which include the breathing and the heartbeat. If the reflected wave from the stationary background can be cancelled and the reflected wave from the subject's body is properly demodulated, the breathing and heartbeat signals of the subject can be extracted. Thus, a human subject buried under the rubble or the debris can be located [18]–[20].

These applications become more interesting if combined with the advantages introduced by the bistatic SAR systems explained in the introduction.

- The use of a bistatic configuration facilitates the use of passive or parasistic receivers. Micro-Doppler extraction can be performed with a relatively inexpensive system without the need to set up a specific mission.
- A passive bistatic system is safe in a military environment. The use of small unmanned aenal vehicles (UAV) receiver and the absence of transmitted signal allows the system to be safer with respect to antiradar missiles and in general without the risk of human lifes.

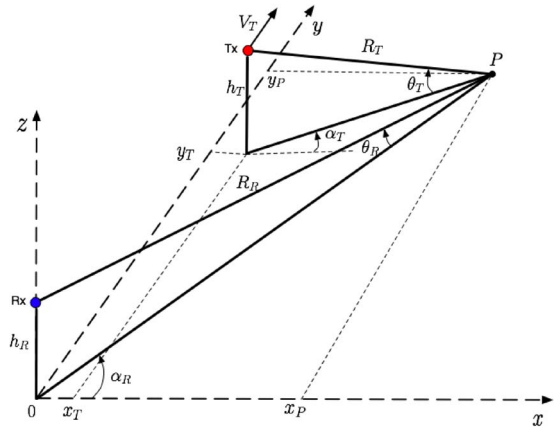

Fig. 1. Bistatic SAR geometry with fixed receiver.

For example, a cheap bistatic SAR system can be deployed using a receiver installed on a hill or a tower to observe and analyze the micro-Doppler from a specific area. Another application is the use of a satellite illuminator and an UAV receiver to perform the micro-Doppler analysis of warfields to recognize what kind of activity in a specific area by the classification of the acquired micro-Doppler signatures (for example to distinguish an air field with helicopters from a farm with farm tractors).

III. Fixed Receiver Bistatic SAR Geometry

In a bistatic SAR, the transmitter and the receiver can have different velocities, altitudes, and flight paths, leading to the possibility of having different acquisition configurations. The simplest case is when both transmitter and receiver have the same velocity and parallel flight paths, while a more complicated configuration exists when the platforms have different velocities and nonparallel flight paths. In the case of a fixed receiver configuration, only the transmitter is moving, and the receiver is fixed. This configuration allows existing monostatic SAR missions to be exploited [7]. In addition, the focusing step is easier, permitting an easier and cheaper test bench to validate new techniques to be extended in the more general bistatic configurations. For these reasons, we choose to perform the first analysis in the field of the micro-Doppler effect in bistatic SAR for this configurations. The considered bistatic geometry is shown in Fig. 1.

At the start of the acquisition (slow time $\eta = 0$), the receiver Rx is located in position $\{0, 0, h_R\}$ while the transmitter Tx is at $\{x_T, y_T, h_T\}$. A point target P in the center of the illuminated scene is located in position $\{x_P, y_P, 0\}$. The range component of the slant range between the receiver and P is $X_R = x_p$, while the range component of the slant range between the transmitter and P is $X_T = x_P - x_T$; the azimuth component of the slant range between the receiver and P is $Y_R = y_P$, while the azimuth component of the slant range at $\eta = 0$ between the transmitter and P is $Y_T = y_P - y_T$. θ_R and θ_T represent the depression angles, while α_R and α_T are the squint angle for the receiver and the transmitter, respectively. The transmitter is moving with velocity V_T in the y direction. Because of the null velocity, the receiver

slant range is $R_R(\eta) = \sqrt{X_R^2 + Y_R^2 + h_R^2}$, while the transmitter slant range is $R_T(\eta) = \sqrt{X_T^2 + (Y_T - \eta V_T)^2 + h_T^2}$, the bistatic slant range history is the sum of the receiver and transmitter slant range histories $R(\eta) = R_T(\eta) + R_R(\eta)$. This is an important factor for the bistatic SAR processing describing the phase history of the received signal.

IV. Micro-Doppler Effect From Vibrating Target in Bistatic Synthetic Aperture Radar (BSAR)

The baseband model of the received bistatic signal from P can be written as [21]:

$$s(\tau,\eta) = A_0 w_r\left(\tau - \frac{R(\eta)}{c}\right) w_{az}(\eta) \exp\left\{-j\frac{2\pi f_0 R(\eta)}{c} + j\pi K_r\left[\tau - \frac{R(\eta)}{c}\right]^2\right\} \quad (1)$$

where τ is the fast time, A_0 is the complex backscatterer coefficient, f_0 is the carrier frequency, K_r is the range chirp rate, $w_r(.)$ is the range envelope, and $w_{az}(.)$ is the composite antenna pattern of the transmitter and receiver. The micro-Doppler effect of interest generally exhibits a dynamic of the same order as the slow time. For this reason, the micromotions will not have appreciable effects in the fast time, and the range compression of (1) can be performed without affecting the analysis. The range compressed signal then results [21]

$$s_{rc}(\tau,\eta) = p_r\left(\tau - \frac{R(\eta)}{c}\right) w_{az}(\eta) \exp\left\{-j\frac{2\pi f_0 R(\eta)}{c}\right\} \quad (2)$$

where $p_r(\tau)$ is the range envelope that includes the amplitude factor.

The point target P has a micromotion radial displacement described by $N(\eta)$. For our purpose, we are assuming that the clutter and a possible constant motion of the target were removed using other processing techniques such as a space-time adaptive processing. In real systems, it is likely that these effect are not removed completely. Consequently, the clutter will be visible in the time-frequency analysis as a constant line, and the target translation will induce a slope on the micro-Doppler signature, making it harder to exploit and interpret the micro-Doppler components.

With these assumptions, the point target P will still have a displacement described by $M(\eta)$ in the range direction. From Fig. 1, the slant range history can be written as

$$R(\eta) = \sqrt{(X_T - N(\eta))^2 + (Y_T - \eta V_T)^2 + h_T^2} + \sqrt{(X_R - N(\eta))^2 + Y_R^2 + h_R^2} = R_T(\eta) + R_R(\eta). \quad (3)$$

The slant range history is directly related to the phase of the received signal in the azimuth direction

$$\Phi(\eta) = \frac{2\pi R(\eta)}{\lambda_c} \quad (4)$$

where λ_c is the carrier wavelength. From the phase history in (4), the instantaneous frequency can be obtained. However, in order to obtain an explicit expression of the different Doppler frequency components, a Taylor series approximation of the slant range is applied, where for orders greater than one, the micromotion effect is assumed to be negligible. The receiver slant range becomes

$$R_R(\eta) \approx \sqrt{X_R^2 + Y_R^2 + h_R^2} - \frac{N'(\eta) X_R \eta}{\sqrt{X_R^2 + Y_R^2 + h_R^2}} = R_{0R} - \frac{N'(\eta)\eta X_R}{R_{0R}}. \quad (5)$$

While the transmitter slant range can be approximated with

$$R_T(\eta) \approx \sqrt{X_T^2 + Y_T^2 + h_T^2} - \frac{(N'(\eta)X_T + V_T Y_T)\,\eta}{\sqrt{X_T^2 + Y_T^2 + h_T^2}} + \frac{V_T^2 \eta^2}{2\sqrt{X_T^2 + Y_T^2 + h_T^2}} = R_{0T} - \frac{(N'(\eta)X_T + V_T Y_T)\,\eta}{R_{0T}} + \frac{V_T^2 \eta^2}{2R_{0T}}. \quad (6)$$

Using (5) and (6), the slant range history (3) can be written

$$R(\eta) \approx R_0 - \left(\frac{N'(\eta)X_R}{R_{0R}} + \frac{N'(\eta)X_T}{R_{0T}}\right)\eta - \frac{V_T Y_T \eta}{R_{0T}} + \frac{V_T^2 \eta^2}{2R_{0T}} \quad (7)$$

where R_{0R} and R_{0T} are the slant ranges for the receiver and the transmitter at the start of the acquisition, and $R_0 = R_{0R} + R_{0T}$, while $N'(\eta)$ represents the istantaneous microvelocity of the target and the product $N'(\eta)\eta$ is the istantaneous target microdisplacement $M(\eta)$.

The expression of $R(\eta)$ in (7) can be separated into two components, a bistatic SAR component, and a target motion component, $R(\eta) \approx R_{BSAR}(\eta) + R_{Target}(\eta)$ where

$$R_{BSAR}(\eta) = R_0 - \frac{V_T Y_T}{R_{0T}}\eta + \frac{V_T^2 \eta^2}{2R_{0T}} \quad (8)$$

$$R_{Target}(\eta) = -\left(\frac{X_R}{R_{0R}} + \frac{X_T}{R_{0T}}\right) M(\eta). \quad (9)$$

Also, the phase history can be divided into two components

$$\Phi(\eta) = \frac{2\pi R(\eta)}{\lambda_c} \approx \frac{2\pi\left(R_{BSAR}(\eta) + R_{Target}(\eta)\right)}{\lambda_c} = \Phi_{BSAR}(\eta) + \Phi_{Target}(\eta). \quad (10)$$

Using the derivative of (10), the instantaneous frequency is obtained as

$$f_D(\eta) = \frac{1}{2\pi}\frac{d}{d\eta}\Phi(\eta) = \frac{1}{2\pi}\frac{d}{d\eta}\Phi_{BSAR}(\eta) + \frac{1}{2\pi}\frac{d}{d\eta}\Phi_{Target}(\eta) = \frac{1}{\lambda_c}\frac{d}{d\eta}R_{BSAR}(\eta) + \frac{1}{\lambda_c}\frac{d}{d\eta}R_{Target}(\eta) = f_{BSAR}(\eta) + f_{MD}(\eta). \quad (11)$$

The instantaneous signal frequency has then two components $f_{BSAR}(\eta)$, a bistatic SAR component and a micro-Doppler component $f_{MD}(\eta)$.

The f_{BSAR} contains the Doppler centroid, the linear, and the quadratic modulation term. This term is known from the geometry and does not affect the micro-Doppler frequency. It is not considered further in the analysis.

The explicit form of $f_{MD}(\eta)$ is

$$f_{MD}(\eta) = -\frac{1}{\lambda_c}\frac{d}{d\eta}\left(\frac{X_R}{R_{0R}} + \frac{X_T}{R_{0T}}\right) M(\eta). \tag{12}$$

Considering a point target P vibrating with a vibration

$$M(\eta) = A_v \cos(w_v \eta) \tag{13}$$

where A_v is the amplitude and w_v is the pulsation of the vibration, respectively, then the micro-Doppler frequency becomes

$$\begin{aligned} f_{MD}(\eta) &= -\frac{1}{\lambda_c} A_v \left(\frac{X_R}{R_{0R}} + \frac{X_T}{R_{0T}}\right) \frac{d}{d\eta}\cos(w_v\eta) \\ &= \frac{1}{\lambda_c} A_v w_v \left(\frac{X_R}{R_{0R}} + \frac{X_T}{R_{0T}}\right) \sin(w_v\eta). \end{aligned} \tag{14}$$

Referring to Fig. 1, the relations between the slant ranges and the angles can be written

$$\begin{aligned} R_{GT} &= \frac{X_T}{\cos(\alpha_T)} = R_{0T}\sin(\theta_T) \Rightarrow \frac{X_T}{R_{0T}} \\ &= \sin(\theta_T)\cos(\alpha_T) \end{aligned} \tag{15}$$

$$\begin{aligned} R_{GR} &= \frac{X_R}{\cos(\alpha_R)} = R_{0R}\sin(\theta_R) \Rightarrow \frac{X_R}{R_{0R}} \\ &= \sin(\theta_R)\cos(\alpha_R) \end{aligned} \tag{16}$$

where R_{GT} and R_{GR} are the ground ranges for the transmitter and the receiver, respectively. Equation (14) can be written in terms of the squint and depression angles

$$\begin{aligned} f_{MD}(\eta) = \frac{1}{\lambda_c} A_v w_v \left(\sin(\theta_R)\cos(\alpha_R)\right. \\ \left. + \sin(\theta_T)\cos(\alpha_T)\right)\sin(w_v\eta). \end{aligned} \tag{17}$$

Equation (17) shows that the micro-Doppler signature depends on the bistatic geometry and is different from the micro-Doppler in the monostatic geometry [14], [15]. A bistatic factor that includes the geometry dependence of the micro-Doppler signature can be defined as

$$\rho = \sin(\theta_R)\cos(\alpha_R) + \sin(\theta_T)\cos(\alpha_T). \tag{18}$$

Then, the micro-Doppler frequency becomes

$$f_{MD}(\eta) = \frac{1}{\lambda_c} A_v w_v \rho \sin(w_v\eta). \tag{19}$$

Equation (19) represents the micro-Doppler signature for a bistatic SAR system that is connected to the signature in the monostatic case [15] through the following equation:

$$f_{MD}(\eta) = \frac{f_{MD_{Mono}}(\eta)\rho}{2}. \tag{20}$$

From (20), it can be seen that for $\rho = 2$, the bistatic signature coincides with the monostatic one.

TABLE I
SIMULATED BISTATIC CONFIGURATION WITH FIXED RECEIVER FOR THE SLANT RANGE HISTORY IN FIG. 2

Tx Velocity	75	m/s
X_T	1600	m
X_R	200	m
Y_T	16	m
Y_R	200	m
h_T	1800	m
h_R	100	m
Acquisition time	0.5	s
Vibration amplitude	0.001	m
Vibration frequency	10	Hz

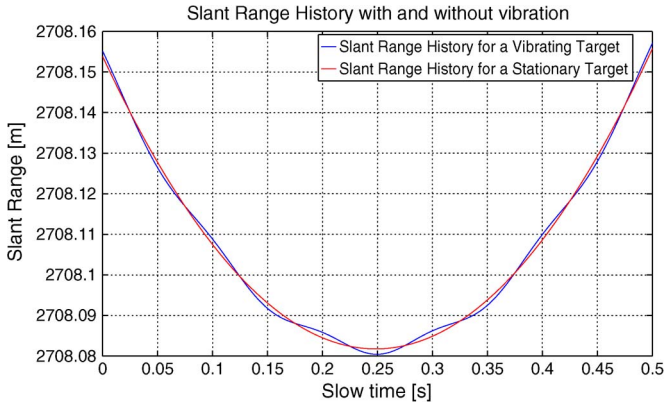

Fig. 2. Slant range history for a vibrating target and for a stationary target.

A. Effect on the Focusing

Using the configuration shown in Table I, an example of the slant range history of a vibrating point target compared with a stationary point target is shown in Fig. 2. The simulated point target is vibrating with a 10-Hz frequency and a 1-mm amplitude. From Fig. 2, the effect of the vibration is evident on the range history for such a small amplitude of the vibration. The phase modulation introduced from the vibration in the signal phase (10) introduces the effect known as paired echoes [12]. The Doppler shift introduced by the vibration creates an infinite number of ghost targets in the focused image, and as in [12], the received signal may be expanded in a series of Bessel function of the first kind

$$J_k(B) = \frac{1}{2\pi}\int_{-\pi}^{\pi} e^{j(B sin w_v\eta - k w_v \eta)} dw_v\eta \tag{21}$$

where $B = (1/\lambda_c)A_v(\sin(\theta_R)\cos(\alpha_R) + \sin(\theta_T)\cos(\alpha_T))$ and $J_k(B)$ decreases with increasing k. Thus, the received signal can be written as

$$\begin{aligned} s_{rc}(\tau,\eta) &= p_r\left(\tau - \frac{R(\eta)}{c}\right) w_{az}(\eta) e^{-j\frac{2\pi f_0 R_{BSAR}(\eta)}{c}} \\ &\quad \times \sum_{k=-\infty}^{\infty} J_k(B) e^{jkw_v\eta} \\ &= p_r\left(\tau - \frac{R(\eta)}{c}\right) w_{az}(\eta) e^{-j\frac{2\pi f_0 R_{BSAR}(\eta)}{c}} \\ &\quad \left[J_0(B) + J_1(B)e^{jw_v\eta} - J_1(B)e^{-jw_v\eta}\right. \\ &\quad + J_2(B)e^{j2w_v\eta} + J_2(B)e^{-j2w_v\eta} \\ &\quad \left. + J_3(B)e^{j3w_v\eta} - J_3(B)e^{-j3w_v\eta} + \ldots\right]. \end{aligned} \tag{22}$$

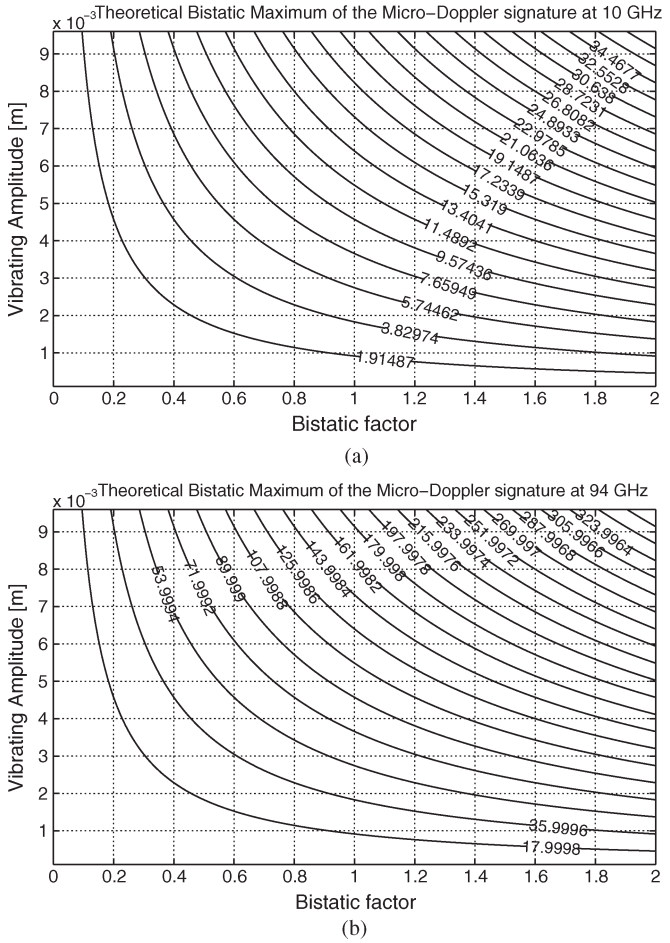

Fig. 3. Maximum amplitude of the micro-Doppler frequency for different bistatic configurations for a vibrating target with a vibrating frequency of 10 Hz and vibrating amplitudes from 0.1 mm to 10 mm. (a) Micro-Doppler for a 10-GHz system. (b) Micro-Doppler for a 94-GHz system. The micro-Doppler is increasing with the increasing vibrating amplitude and bistatic factor.

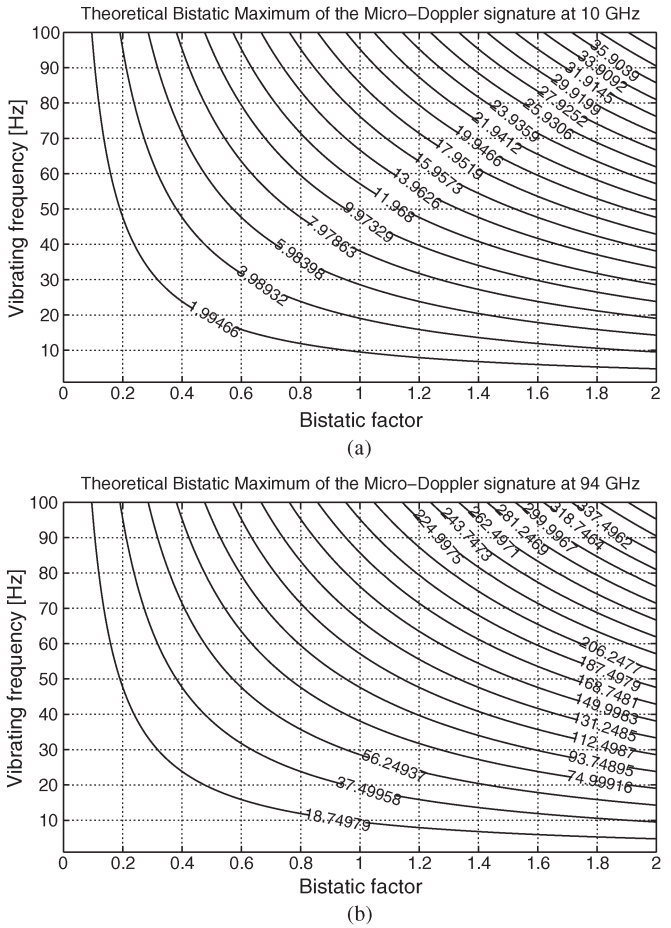

Fig. 4. Maximum amplitude of the micro-Doppler frequency for different bistatic configurations for a vibrating target with a vibrating amplitude of 1 mm and vibrating frequencies from 1 Hz to 100 Hz. (a) Micro-Doppler for a 10-GHz system. (b) Micro-Doppler for a 94-GHz system. The micro-Doppler is increasing with the increasing vibrating frequency and bistatic factor.

Unlike [12], the amplitude factor of the ghost scatterers, represented by $J_k(B)$, depends on the bistatic SAR geometry. Thus, depending on the particular geometry, the effect on the focused image of a particular vibrating target will be more or less evident.

B. Effect of the Bistatic Factor

In this section, the effect of the bistatic configuration on the amplitude values of the induced micro-Doppler is analyzed. The amplitude of the vibration can be obtained from the measured maximum of the micro-Doppler signature using (19) as

$$A_v = \frac{\lambda_c \max\left(f_{MD}(\eta)\right)}{w_v \rho}. \tag{23}$$

The difference between (23) and that in [15] for the monostatic case is the dependence on the bistatic factor ρ. This dependence must be considered in the micro-Doppler signature analysis in order to correctly identify the amplitude of the vibration. Different acquisition geometries induce different micro-Doppler amplitudes, and thus a good knowledge of the geometry is required in order to obtain the amplitude of the vibration. In Fig. 3(a) and in Fig. 3(b), the theoretical bistatic maximum of the micro-Doppler signature for a 94-GHz and a 10-GHz system, respectively, for a vibrating target with $w_v = 20\pi$ rad/sec and a vibration amplitude from 0.1 mm to 10 mm are shown. The amplitude of the micro-Doppler signature depends also on the vibrating frequency w_v as can be seen in (23). In Fig. 4(a) and (b), the theoretical bistatic maximum of the micro-Doppler signature with a 94-GHz and a 10-GHz system for a vibrating target with 1 mm of vibrating amplitude and with a vibrating frequency from 1 Hz to 100 Hz are shown. For both cases, the bistatic factor influences the amplitude of the micro-Doppler signature. This factor is the sum of the conic angle of the transmitter and receiver and therefore is dependent on the BSAR geometry. From both Figs. 3 and 4, the bistatic factor influences the amplitude of the micro-Doppler signature, when $\rho = 2$ the curves assumes the maximum values and they coincide with the maximum micro-Doppler obtained in a monostatic case.

This aspect must be considered because a certain amplitude of the micro-Doppler signature corresponds to a family of vibrating amplitudes. The correct amplitude can be obtained only with the knowledge of the bistatic factor. In addition, the amplitude is also influenced by the carrier frequency. For example, a 10-GHz system would not be able to detect

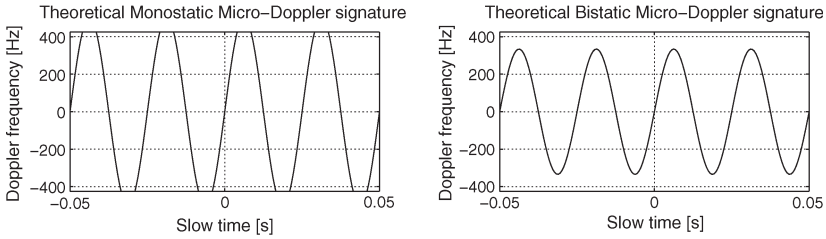

Fig. 5. Theoretical micro-Doppler signature for a target vibrating at 40 Hz width 3 cm of amplitude from a X-band system with 950 Hz of azimuth Doppler bandwidth. (a) Monostatic case running over the azimuth Doppler bandwidth. (b) Bistatic case with the entire signature visible in the azimuth Doppler bandwidth.

micro-Doppler signatures generated by very small motions. Furthermore, larger micromotions will introduce aliasing if not correctly sampled in a 94-GHz system. For this reason, this is an important aspect in the design and the choice of the measurement system.

The bistatic factor offers an advantage in the use of a bistatic configuration with respect to the monostatic configuration for larger vibration frequencies and amplitudes. From (19), it is seen that the bistatic factor reduces the amplitude of the micro-Doppler signature compared with the one obtained for the same vibration in the monostatic case. This means that for vibrations introducing high Doppler shifts, running over the azimuth Doppler bandwidth in the monostatic case, the analysis of the signature can suffer from aliasing. However, as the use of a bistatic configuration reduces the micro-Doppler amplitude, it is possible to keep the signature inside the azimuth Doppler bandwidth. This means that it is possible to use a smaller minumum PRF to avoid aliasing in the analysis compared to the monostatic configuration. Fig. 5 shows an example of a bistatic configuration for the analysis in X-band of a 40-Hz vibrating target with 3 cm of vibrating amplitude. In Fig. 5(a), the monostatic micro-Doppler signature runs over the limit given by the Doppler bandwidth making the analysis of the signature impossible, while Fig. 5(b) shows the same vibration analyzed from a bistatic system. In this case, the bistatic factor ρ is weighting the micro-Doppler signature, keeping it inside the Doppler bandwidth.

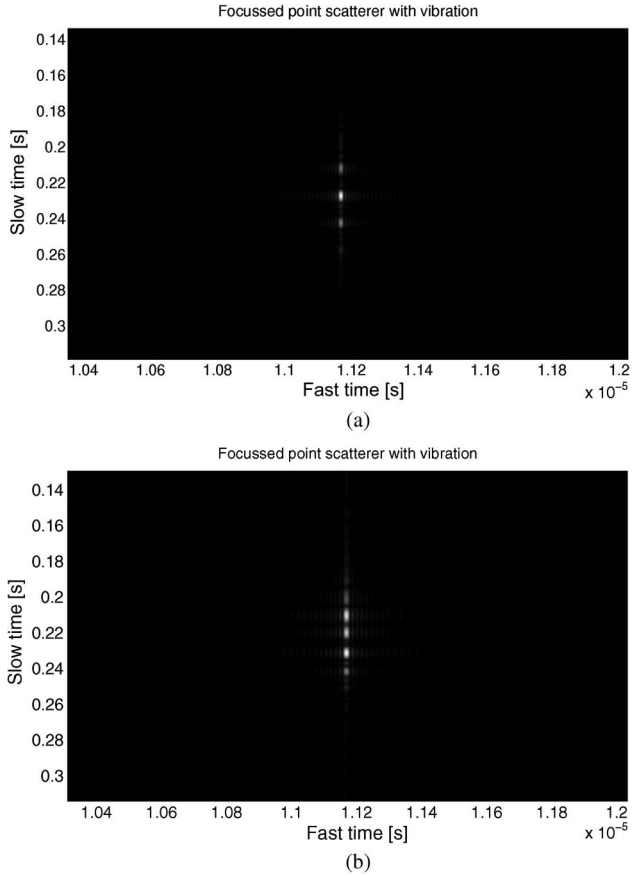

Fig. 6. Focused point targets in a bistatic SAR system with fixed receiver. The vibrating amplitude is 0.5 mm, and the vibration frequency is 10 Hz. In (a), the results are shown for a transmitter at 2100 m of altitude, while in (b), the results show the result for the transmitter at 900 m. In (a), the number of ghost scatterers is smaller than in (b).

V. Simulation Results

Vibrating targets were simulated and their micro-Doppler signatures from a bistatic SAR system analyzed. First, the effect of the vibration on the focused image (Section IV-A) is shown. The different micro-Doppler signatures are then analyzed for different bistatic configurations for systems working with a carrier frequency of 10 and 94 GHz. The two frequencies were chosen because theoretically they produce results that demonstrate that it is possible to detect micro-Doppler signatures of interest such as engines and humans. In addition, X-band radar are very common [22], [23], and some 94-GHz radar are operational like MEMPHIS [24].

A. Effect on Focussing

The result of bistatic focusing for two different configurations with transmitter altitudes of 2100 and 900 m are shown for a 94-GHz system in Fig. 6(a) and (b), respectively. These two altitudes were chosen to highlight the effect of the different geometry on the focused image. The simulated point target is vibrating at 10 Hz with an amplitude of 0.5 mm. The resulting focused images in both cases show the presence of ghost scaterers along the azimuth direction on both sides of the point scatterer. However, the same vibration exhibits a different number of ghost scatterers with different amplitudes for both configurations. This aspect can be analyzed and confirmed using the discussion in Section IV-A. For the first configuration, Fig. 6(a), the bistatic scale factor is 1.0143, and the value of B in (22) is 0.9984, while in the simulation shown in Fig. 6(b), the bistatic scale factor is 1.5382 and

TABLE II
COMPUTED VALUES OF THE FIRST KIND BESSEL FUNCTION FOR THE TWO CONFIGURATIONS

Order of $J_k(B)$	Config. (a)	Config. (b)
0	0.7659	0.5039
1	0.4395	0.5599
2	0.1146	0.2356
3	0.0195	0.0625

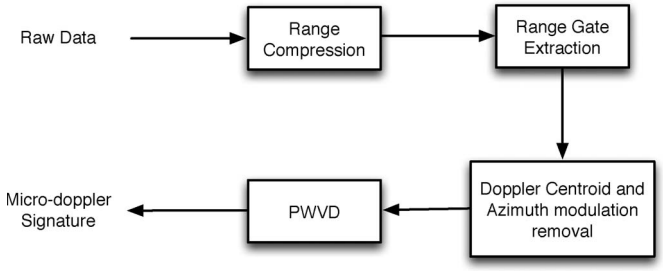

Fig. 7. Steps for the extraction of the micro-Doppler signature from the simulated data.

$B = 1.5141$. With these values, the Bessel function of the first kind $J_k(B)$ can be computed for both configurations. These values are weighting the amplitude of the scatterer and the ghost scatterers. The computed values of the first four orders of $J_k(B)$ for the two configurations are shown in Table II. The values of $J_k(B)$ in Table II confirm that for the configuration simulated in Fig. 6(a), the amplitude of the real point scatterer is higher than those for the ghost scatterers pairs, while for the configuration in Fig. 6(b), the amplitude of the ghost scatterers is greater than the real point scatterers for the first pair of ghosts.

B. Micro-Doppler Signature Analysis From Simulated Data

Fig. 7 shows a block diagram of the steps needed to perform the time-frequency analysis of the micro-Doppler signature for a bistatic SAR with fixed receiver. Starting from the raw data, the range compression step is performed using a replica of the transmitted signal. From the range compressed data, the range gate containing the scatterer is selected. For the configurations analyzed in this work, the range migration is contained within a fraction of the resolution cell; however, in the presence of a larger range migration, a range cell migration correction [25] step can be performed before the extraction of the range gate.

In order to align the signal within the time-frequency plane to obtain a correct visualization and positioning of the time-frequency distribution, the Doppler centroid and the azimuth frequency slope is removed from the signal before the computation of the Pseudo Wigner Ville Distribution (PWVD) [16], which is used to extract the micro-Doppler signature of the target.

Using this analysis procedure, vibrating targets in bistatic SAR configurations with 10-GHz and 94-GHz systems were analyzed and compared with the results obtained using a monostatic configuration, and the theoretical micro-Doppler. Fig. 8 shows the PWVDs of the received SAR signal for a 94 GHz system for a point target vibrating at 10 Hz with an amplitude of the vibration of 1 mm. Fig. 8(a) and (c) show the PWVD

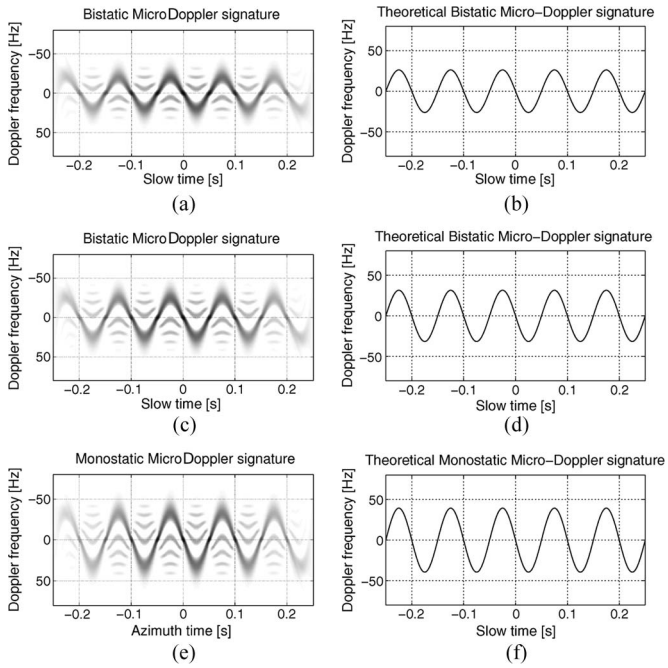

Fig. 8. Micro-Doppler signatures of a vibrating target with 10 Hz of vibration and 1 mm of amplitude on a 94 GHz system. (a) and (c) show the analyzed PWVD of the two bistatic configurations shown in Table III, while (e) shows the micro-Doppler signature in the monostatic case. (b), (d), and (f) show the theoretical signature for (a), (c), and (e), respectively.

TABLE III
SIMULATED BISTATIC CONFIGURATIONS FOR THE SIMULATED TARGET IN FIG. 8

	Configuration 1	Configuration 2	Monostatic
Carrier Frequency	94 GHz	94 GHz	94 GHz
Tx Velocity	75 m/s	75 m/s	75 m/s
Acquisition Time	0.5 s	0.5 s	0.5 s
Vibration Amplitude	0.001 m	0.001 m	0.001 m
Vibration Frequency	10 Hz	10 Hz	10 Hz
X_T	1600 m	1600 m	-
Y_T	19 m	19 m	-
h_T	1800 m	1800 m	-
X_R	200 m	600 m	-
Y_R	200 m	200 m	-
h_R	100 m	100 m	-
Bistatic Factor	**1.3310**	**1.6014**	**2**

obtained with the two bistatic configurations in Table III, while Fig. 8(e) shows the PWVD in the monostatic case for the same target. Fig. 8(b), (d), and (f) shows the theoretical micro-Doppler signature for the cases analyzed in Fig. 8(a), (c), and (e), respectively. Table III gives the two bistatic configurations and the monostatic configuration used in the simulation shown in Fig. 8. It can be seen that the only difference resides in the geometry and therefore the bistatic factor that influences the micro-Doppler signature.

From Fig. 8, it is confirmed that the analyzed bistatic micro-Doppler signatures match those expected from theory. The frequency of the vibration can be measured by inspection the PWVDs confirming the 10 Hz simulated vibration. The measured micro-Doppler amplitude for the first configuration is 26 Hz. Equation (23) yields an estimated vibrating amplitude of 9.9985×10^{-4} m which is close to the simulated 1-mm

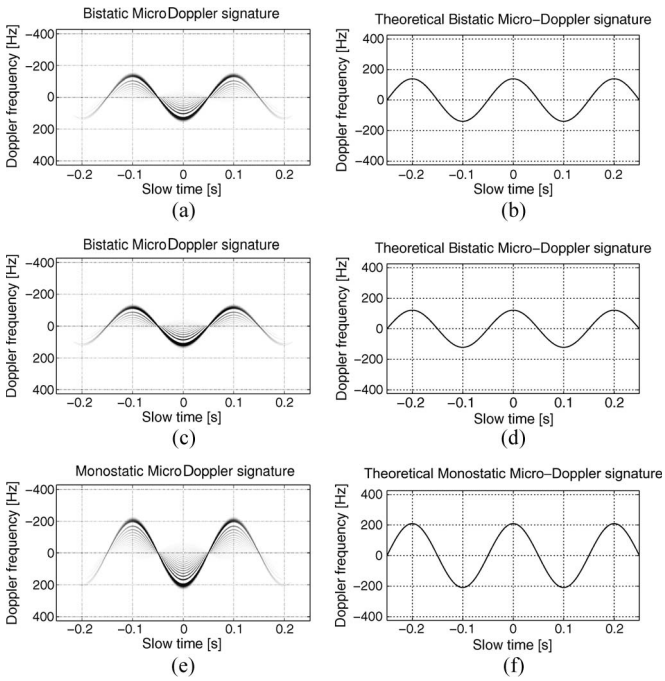

Fig. 9. Micro-Doppler signatures of a vibrating target with 5 Hz of vibration and 0.1 m of amplitude on a 10-GHz system. (a) and (c) show the analyzed PWVD of the two bistatic configurations shown in Table IV, while (e) shows the micro-Doppler signature in the monostatic case. (b), (d), and (f) show the theoretical signature for (a), (c), and (e), respectively.

vibration amplitude. This is confirmed using the maximum of the theoretical micro-Doppler of 26.2 Hz obtained using (19). In the second configuration, the measured micro-Doppler amplitude is 32 Hz yielding an estimated vibration amplitude of 1.01×10^{-3} m. The original 1-mm amplitude can be obtained from the maximum of the theoretical micro-Doppler that is 31.5 Hz. As expected both the bistatic micro-Doppler exhibits a maximum of the micro-Doppler signature smaller than the monostatic case which is of 39.37 Hz.

Fig. 9 shows the PWVDs of the received SAR signal for a 10-GHz system for a point target vibrating at 5 Hz with an amplitude of the vibration of 0.1 m. Fig. 9(a) and (c) shows the PWVD obtained with the two bistatic configurations in Table IV, while Fig. 9(e) shows the PWVD in the monostatic case for the same target. Fig. 9(b), (d), and (f) shows the theoretical micro Doppler signature for the cases analyzed in Fig. 9(a), (c), and (e), respectively. Table IV reports the two bistatic configurations and the monostatic configuration used in the simulation shown in Fig. 9. Fig. 9 shows the results for the 10-GHz simulations. The measured micro-Doppler amplitude for the first configuration is 140 Hz yielding an estimated vibrating amplitude of 0.1004 m from (23). This is close to the simulated 0.1-m vibration amplitude and confirmed using the maximum of the theoretical micro-Doppler of 139.38 Hz obtained using (19). In the second configuration, the measured micro-Doppler amplitude is 125 Hz, yielding an estimated vibration amplitude of 0.102 m. The original 0.1-m amplitude is computed from the maximum of the theoretical micro-Doppler amplitude that is 121.76 Hz. The maximum amplitude of the micro-Doppler in the monostatic case which is of 209.43 Hz.

TABLE IV
SIMULATED BISTATIC CONFIGURATIONS FOR THE SIMULATED TARGET IN FIG. 9

	Configuration 1	Configuration 2	Monostatic
Carrier Frequency	10 GHz	10 GHz	10 GHz
Tx Velocity	75 m/s	75 m/s	75 m/s
Acquisition Time	0.5 s	0.5 s	0.5 s
Vibration Amplitude	0.1 m	0.1 m	0.1 m
Vibration Frequency	5 Hz	5 Hz	5 Hz
X_T	1600 m	1600 m	-
Y_T	19 m	19 m	-
h_T	1800 m	2800 m	-
X_R	200 m	600 m	-
Y_R	200 m	200 m	-
h_R	100 m	100 m	-
Bistatic Factor	**1.3310**	**1.1627**	**2**

These results demonstrate that the micro-Doppler signature for a specific configuration changes with the bistatic acquisition geometry. This is an important factor to be considered in the classification and recognition of targets characterized by a particular micro-Doppler signature. In addition, (20) can be used to exploit existing micro-Doppler signatures in a bistatic environment.

VI. CONCLUSION

In this paper, micro-Doppler signatures from vibrating targets in bistatic SAR systems were investigated. The bistatic configuration with a fixed receiver was used to derive an expression for the bistatic micro-Doppler signature. The effect on the focused image was also analyzed. The bistatic case shows a substantial difference to that of the traditional monostatic case. The bistatic micro-Doppler signature is influenced by the bistatic geometry. Vibrating targets were simulated to confirm the theoretical analysis on the focused image and on the micro-Doppler signatures. The simulations confirmed the model that provides a useful tool for the analysis of the micro-Doppler signature from a bistatic SAR system. The effect of the bistatic factor must be considered for target classification and recognition.

It was demonstrated that the bistatic configuration exhibits the advantage of a reduced minimum required PRF compared to that required in the monostatic SAR. Furthermore, this reduces the effects of potential aliasing in the analysis of the micro-Doppler signature compared to the monstatic case. It was shown that this is due to the effect of the bistatic geometry on the maximum amplitude of the micro-Doppler signature that is seen to be equal or less to the amplitude of the micro-Doppler signature in the monostatic case. Thus, for a family of micro-Doppler effects and a fixed PRF, the analysis from a monostatic geometry will appear aliased, while the use of a bistatic configuration could prevent aliasing. Thus, the bistatic configuration facilitates the analysis of a wider range of signatures with respect to the monostatic system.

ACKNOWLEDGMENT

The authors would also like to acknowledge the anonymous reviewers for their useful comments and suggestions.

REFERENCES

[1] M. Cherniakov, *Bistatic Radar: Emerging Technology*. Hoboken, NJ: Wiley, 2008.

[2] I. Walterscheid, T. Espeter, A. Brenner, J. Klare, J. Ender, H. Nies, R. Wang, and O. Loffeld, "Bistatic SAR experiments with PAMIR and TerraSAR-X-setup, processing, and image results," *IEEE Trans. Geosci. Remote Sens.*, vol. 48, no. 8, pp. 3268–3279, Aug. 2010.

[3] M. Zink, G. Krieger, H. Fiedler, I. Hajnsek, A. Moreira, and M. Werner, "TanDEM-X—The first bistatic SAR formation in space," in *Proc. ARSI ESA/ESTEC*, Noordwijk, The Netherlands, 2006.

[4] G. Yates and A. Horne, "Bistatic SAR image formation," in *Proc. EUSAR*, Ulm, Germany, 2004.

[5] M. Antoniou, R. Saini, and M. Cherniakov, "Results of a space-surface bistatic SAR image formation algorithm," *IEEE Trans. Geosci. Remote Sens.*, vol. 45, no. 11, pp. 3359–3371, Nov. 2007.

[6] A. Goh, M. Preiss, N. Stacy, and D. Gray, "Bistatic SAR experiment with the Ingara imaging radar," *IET Radar, Sonar Navig.*, vol. 4, no. 3, pp. 426–437, Jun. 2010.

[7] S. Duque, P. Lopez-Dekker, and J. Mallorqui, "Single-pass bistatic SAR interferometry using fixed-receiver configurations: Theory and experimental validation," *IEEE Trans. Geosci. Remote Sens.*, vol. 48, no. 6, pp. 2740–2749, Jun. 2010.

[8] S. Duque, P. Lopez-Dekker, J. Merlano, and J. Mallorqui, "Bistatic SAR along track interferometry with multiple fixed receivers," in *Proc. IEEE IGARSS*, 2010, pp. 4099–4102.

[9] M. Davis and R. Kapfer, "Bistatic SAR using illumination from a tethered ground moving target indication radar," in *Proc. IEEE Radar Conf.*, May 2009, pp. 1–6.

[10] D. Cerutti-Maori and J. Ender, "Performance analysis of multistatic configurations for spaceborne GMTI based on the auxiliary beam approach," *Proc. Inst. Elect. Eng.—Radar Sonar Navig.*, vol. 153, no. 2, pp. 96–103, Apr. 2006.

[11] X. Li, B. Deng, Y. Qin, H. Wang, and Y. Li, "The influence of target micromotion on SAR and GMT," *IEEE Trans. Geosci. Remote Sens.*, vol. 49, no. 7, pp. 2738–2751, Jul. 2011.

[12] V. Chen, F. Li, S.-S. Ho, and H. Wechsler, "Micro-Doppler effect in radar: Phenomenon, model, and simulation study," *IEEE Trans. Aerosp. Electron. Syst.*, vol. 42, no. 1, pp. 2–21, Jan. 2006.

[13] V. Chen, *Micro-Doppler Effect in Radar*, 1st ed. Norwood, MA: Artech House, 2011.

[14] T. Sparr and B. Krane, "Micro-Doppler analysis of vibrating targets in SAR," *Proc. Inst. Elect. Eng.—Radar Sonar Navig.*, vol. 150, no. 4, pp. 277–283, Aug. 2003.

[15] M. Ruegg, E. Meier, and D. Nuesch, "Vibration and rotation in millimeter-wave SAR," *IEEE Trans. Geosci. Remote Sens.*, vol. 45, no. 2, pp. 293–304, Feb. 2007.

[16] L. Cohen, "Time-frequency distributions-a review," *Proc. IEEE*, vol. 77, no. 7, pp. 941–981, Jul. 1989.

[17] L. Zheng and S. Hui-xia, "Micro-Doppler analysis and application of radar targets," in *Proc. ICIA*, Jun. 2008, pp. 1343–1347.

[18] K.-M. Chen, Y. Huang, J. Zhang, and A. Norman, "Microwave life-detection systems for searching human subjects under earthquake rubble or behind barrier," *IEEE Trans. Biomed. Eng.*, vol. 47, no. 1, pp. 105–114, Jan. 2000.

[19] S. Ram, C. Christianson, Y. Kim, and H. Ling, "Simulation and analysis of human micro-dopplers in through-wall environments," *IEEE Trans. Geosci. Remote Sens.*, vol. 48, no. 4, pp. 2015–2023, Apr. 2010.

[20] A. Sume, M. Gustafsson, M. Herberthson, A. Janis, S. Nilsson, J. Rahm, and A. Orbom, "Radar detection of moving targets behind corners," *IEEE Trans. Geosci. Remote Sens.*, vol. 49, no. 6, pp. 2259–2267, Jun. 2011.

[21] Y. L. Neo, "Digital processing algorithms for bistatic synthetic aperture radar data," Ph.D. dissertation, Univ. British Columbia, Vancouver, BC, Canada, 2007.

[22] A. Kinghorn and A. Nejman, "PicoSAR—An advanced lightweight SAR system," in *Proc. EuRAD*, 2009, pp. 168–171.

[23] J. Ender and A. Brenner, "PAMIR—A wideband phased array SAR/MTI system," *Proc. Inst. Elect. Eng.—Radar Sonar Navig.*, vol. 150, no. 3, pp. 165–172, Jun. 2003.

[24] H. Schimpf, H. Essen, S. Boehmsdorff, and T. Brehm, "MEMPHIS-a fully polarimetric experimental radar," in *Proc. IEEE IGARSS*, Jun. 2002, vol. 3, pp. 1714–1716.

[25] I. Cumming and F. Wong, *Digital Processing of Synthetic Aperture Radar Data: Algorithms and Implementation*, 1st ed. Norwood, MA: Artech House, 2005.

Carmine Clemente (S'09) received the Laurea (*cum laude*) and Laurea Specialistica (*cum laude*) degrees in telecommunications engineering from Universita' degli Studi del Sannio, Benevento, Italy, in 2006 and 2009, respectively. He is currently working toward the Ph.D. degree in the Department of Electronic and Electrical Engineering, University of Strathclyde, Glasgow, U.K.

From February 2008 to September 2009 he worked at the Interdipartmental Centre of Technologies (TEDASS)—Universita' degli Studi del Sannio, Benevento, Italy working in the field of satellite data processing for polar-orbiting active and passive sensors, in particular working on high-performance computing for remote sensing applications. His research interest include synthetic aperture radar (SAR) focusing algorithms development, bistatic SAR focusing, micro-Doppler signature analysis and extraction from multistatic radar platforms, statistical signal processing, and high-perfomance computing.

John J. Soraghan (S'84–M'86–SM'96) received the B.Eng. (Hons.) and M.Eng.Sc. degrees in electronic engineering from University College Dublin, Dublin, Ireland, in 1978 and 1983, respectively, and the Ph.D. degree in electronic engineering from the University of Southampton, Southampton, U.K., in 1989. His doctoral research focused on synthetic aperture radar (SAR) processing on the distributed array processor.

After graduating, he worked with the Electricity Supply Board in Ireland and with Westinghouse Electric Corporation in the U.S. In 1986, he joined the Department of Electronic and Electrical Engineering, University of Strathclyde, Glasgow, U.K., as a Lecturer and became a Senior Lecturer in 1990, a Reader in 2000, and a Professor in signal processing in September 2003, within the Institute for Communications and Signal Processing (ICSP). In December 2005, he became the Head of the ICSP. He currently holds the Texas Instruments Chair in Signal Processing with the University of Strathclyde. He was a Manager of the Scottish Transputer Centre from 1988 to 1991, and a Manager of the DTI Parallel Signal Processing Centre from 1991 to 1995. His main research interests are signal processing theories, algorithms, and architectures with applications to remote sensing, telecommunications, biomedicine, and condition monitoring.

Dr. Soraghan is a member of the Institution of Engineering and Technology.